Check for updates

OPEN

Global analysis of protein degradation in prion infected cells

Charles R. Hutti[1], Kevin A. Welle[2], Jennifer R. Hryhorenko[2] & Sina Ghaemmaghami[1,2✉]

Prion diseases are rare, neurological disorders caused by the misfolding of the cellular prion protein (PrP^C) into cytotoxic fibrils (PrP^{Sc}). Intracellular PrP^{Sc} aggregates primarily accumulate within late endosomes and lysosomes, organelles that participate in the degradation and turnover of a large subset of the proteome. Thus, intracellular accumulation of PrP^{Sc} aggregates has the potential to globally influence protein degradation kinetics within an infected cell. We analyzed the proteome-wide effect of prion infection on protein degradation rates in N2a neuroblastoma cells by dynamic stable isotopic labeling with amino acids in cell culture (dSILAC) and bottom-up proteomics. The analysis quantified the degradation rates of more than 4,700 proteins in prion infected and uninfected cells. As expected, the degradation rate of the prion protein is significantly decreased upon aggregation in infected cells. In contrast, the degradation kinetics of the remainder of the N2a proteome generally increases upon prion infection. This effect occurs concurrently with increases in the cellular activities of autophagy and some lysosomal hydrolases. The resulting enhancement in proteome flux may play a role in the survival of N2a cells upon prion infection.

Prion diseases are infectious neurodegenerative disorders associated with the cytotoxic aggregation of the prion protein (PrP)[1–3]. These diseases are present in a number of mammalian species and include scrapie in sheep, bovine spongiform encephalopathy in cattle, and chronic wasting disease in deer. In humans, prion diseases include kuru, Creutzfeldt–Jakob disease, fatal familial insomnia, and Gerstmann–Straussler–Scheinker syndrome[4,5]. During the course of each of these diseases, aggregates of the prion protein (PrP^{Sc}) accumulate and cause the conversion of the non-toxic cellular form of the prion protein (PrP^C) into additional PrP^{Sc} in a self-seeding fashion[6]. While the function of PrP^C remains controversial, PrP^{Sc} is thought to be the sole cause of prion diseases.

In uninfected cells, the prion protein resides primarily on the cell surface and is degraded through the endocytic pathway as part of its natural turnover cycle[7–9]. While PrP^C is readily degraded by lysosomal hydrolases, PrP^{Sc} appears to be more resistant to proteolysis and accumulates within endosomal and lysosomal compartments during the course of infection[7,10,11]. Over time, PrP^{Sc} accumulates intracellularly and may contribute to cell death and dispersion of aggregates into the extracellular space[12]. Prion aggregates can cause the conversion of PrP^C on adjacent cells, thus spreading PrP^{Sc} aggregates throughout the brain. While the exact mechanism of pathogenicity remains under active study, the accumulation of PrP^{Sc} in the lysosome and endosomal vesicles is thought to contribute to the cytotoxicity of prions[13].

The lysosome serves as a proteolytic center for two major protein degradation pathways within the cell: autophagy and endosome-mediated degradation[14,15]. Lysosomal vesicles facilitate the hydrolysis of proteins into their constitutive amino acids by subjecting them to low pH unfolding conditions and acidic hydrolases. Given that PrP^{Sc} accumulates in the lysosome during the course of prion infection, several studies have investigated the direct and indirect effects of accumulating prion aggregates on lysosomal degradation[13]. In mouse brains infected with prion aggregates, the expression of lysosomal hydrolases are upregulated at the level of transcription[16]. Similarly, in cultured N2a cells, the activities of lysosomal hydrolases have been shown to be upregulated during prion infection[17]. In both mouse and hamster brains infected with prion aggregates, there are increases in the abundances of autophagy-related proteins p62/SQSTM1 and LC3–II[18]. While increases in the abundances of p62/SQSTM1 and LC3–II can also be interpreted as markers of late-stage autophagic inhibition, N2a cells exhibit increased expression of p62/SQSTM1 mRNA, supporting the hypothesis that autophagy is upregulated upon prion infection. Together, these studies suggest that host cells upregulate lysosomal degradation as a response to prion infection. However, other studies have provided evidence suggesting that accumulation of prion aggregates inhibits lysosomal degradation by interfering with the ability of the cell to endocytose and degrade proteins[19].

[1]Department of Biology, University of Rochester, New York 14627, USA. [2]University of Rochester Mass Spectrometry Resource Laboratory, New York 14627, USA. ✉email: sina.ghaemmaghami@rochester.edu

Considering these opposing effects of prion infection on intracellular protein degradation, the net effect of PrP^{Sc} accumulation on global protein turnover kinetics remains unclear. Thus, we sought to utilize a proteomic approach to conduct a global analysis of changes in protein degradation kinetics during prion infection.

Recent advances in quantitative mass spectrometry and bottom-up proteomics have enabled the measurement of protein turnover kinetics on a global scale[20–22]. These studies have shown that protein half-lives can range from minutes to years and can be influenced by several intrinsic and extrinsic factors. As examples, the presence of specific degradation sequence motifs (degrons), as well as a protein's physical properties such as isoelectric points, surface area, thermodynamic stabilities, and molecular weights can influence a protein's inherent half-life[23–28]. Additionally, the relative activities of specific protein degradation pathways such as autophagy and the ubiquitin proteasome system (UPS) can influence the degradation kinetics of specific subsets of the proteome[29–32]. By using modern proteomic techniques such as dynamic stable isotopic labeling of amino acids in cell culture (dSILAC), the in vivo degradation rate of individual proteins within the proteome can be measured in different cellular and environmental conditions[32,33]. In this study, we used dSILAC to investigate the proteome-wide impact of intracellular PrP^{Sc} accumulation on protein clearance kinetics in prion infected cells.

Results

Measurement of degradation kinetics by dSILAC.
An overview of the dSILAC methodology used in this study is illustrated in Fig. 1A and details of the experimental design are described in "Methods". Briefly, cells are cultured in media containing isotopically labeled amino acids (^{13}C-lysines and ^{13}C-arginines). The rate by which unlabeled ("light") proteins within the cell are replaced by newly synthesized labeled ("heavy") proteins can be quantified by mass spectrometry over time. The quantified rate constant for fractional labeling is commonly referred to as the protein clearance rate ($k_{clearance}$)[21,34]. The measurement of $k_{clearance}$ can be conducted on proteome-wide scales using tandem mass spectrometry and a bottom-up proteomic workflow[35]. In dividing cells, measured rates of protein clearance represent the additive effects of two factors: protein degradation ($k_{degradation}$) and protein dilution due to cell division ($k_{division}$) (Fig. 1B). Thus, degradation rate constants can be obtained by subtracting experimentally determined rates of cell division from rates of clearance[21,36].

Prion infected and uninfected cultured cell models.
For our analysis, we utilized a transgenic clone of N2a neuroblastoma cells that highly overexpress the PrP gene (N2a-Cl3)[37,38]. When infected with the Rocky Mountain Laboratories (RML) prion strain, these cells accumulate protease-resistant PrP^{Sc} at cellular levels that are equivalent to terminal prion infected brain tissues[37]. As a transformed cell line, N2a cells are known to have an unstable karyotype. Thus, to obtain an uninfected control that was minimally genetically divergent, prion infected cells were treated with the anti-prion compound quinacrine[39,40]. We cleared populations of infected N2a-Cl3 cells of PrP^{Sc} by treating them with a standard dosage of quinacrine for four weeks and confirmed the clearance of protease-resistant PrP^{Sc} by western blots (Fig. 2A). We further demonstrated that prion-cleared cells remained infectible by PrP^{Sc} through exposure to ScN2a-Cl3 extracts (Fig. 2A). Thus, although we cannot rule out the possibility that selection of specific cell populations occurred under quinacrine treatment, prion-cleared cells remain susceptible to prion propagation upon reinfection. Prior to isotopic labeling, prion-cleared controls were propagated in the absence of quinacrine for one week in order to remove any potentially confounding effects of quinacrine in the media. Prion infected and cleared N2a-Cl3 cells will be referred to as −QA and +QA, respectively.

The clearance kinetics of the prion protein in −QA and +QA cells.
We conducted dSILAC analyses on −QA and +QA cells and were able to quantify the clearance kinetics of 58,590 peptides mapped to 5,215 proteins in −QA cells and 59,320 peptides mapped to 5,168 proteins in +QA cells (Table 1). 4,730 proteins were shared between the two datasets. We initially focused on analyzing the kinetic data mapped to PrP. We observed that $k_{clearance}$ of the total prion protein population was faster in +QA cells in comparison to −QA cells (Fig. 2B). Measured $k_{clearance}$ values for PrP in +QA and −QA cells were 1.22 day^{-1} and 0.99 d^{-1}, respectively. The degradation rate of PrP^{C} in dividing cells was calculated as 0.70 day^{-1} by subtracting the rate of cell division from the clearance rate. The slower rate of PrP clearance in −QA cells is consistent with the fact that PrP^{Sc} aggregates are partially resistant to cellular proteolysis and thus have a slower degradation rate than PrP^{C}.

However, this analysis is complicated by the fact that both PrP^{C} and PrP^{Sc} are present in −QA cells, and peptides from both populations are simultaneously quantified and contribute to the observed fractional labeling. Thus, in order to measure the degradation rate of PrP^{Sc} alone, a second dSILAC experiment was performed where lysates were treated with proteinase K (PK) and the protease-resistant PrP^{Sc} was isolated by phosphotungstic acid (PTA) precipitation[41] prior to LC–MS/MS analysis (Fig. 2C). PrP data from this experiment established the $k_{clearance}$ of PrP^{Sc} in dividing N2a cells as 0.62 d^{-1}. Importantly, this rate of clearance exactly mirrors the measured rate of cell division in these cells (Fig. 2C). This observation suggests that the degradation of PrP^{Sc} in dividing prion infected cells is inhibited to such an extent that its clearance occurs almost entirely by cellular dilution rather than degradation.

If prion clearance in dividing cells occurs primarily by dilution due to cell division, then the arrest of cell division should substantially decrease the observed $k_{clearance}$ of PrP^{Sc}. To test this hypothesis, a third dSILAC experiment was performed where cell division was arrested 48 h prior to the introduction of ^{13}C lysine/arginine by the addition of sodium butyrate, which has been shown to arrest cell division and induce the differentiation of N2A cells to neuron-like cells[42–45]. Labeled extracts from sodium butyrate-treated division-arrested cells were treated with PK and protease-resistant PrP^{Sc} was isolated by PTA precipitation prior to LC–MS/MS analysis (Fig. 2D). As predicted, we observed that the clearance rate of PrP^{Sc} in division arrested cells (0.36 day^{-1}) is significantly slower than that found in dividing cells. Together, this data confirms that the clearance of PrP in prion infected
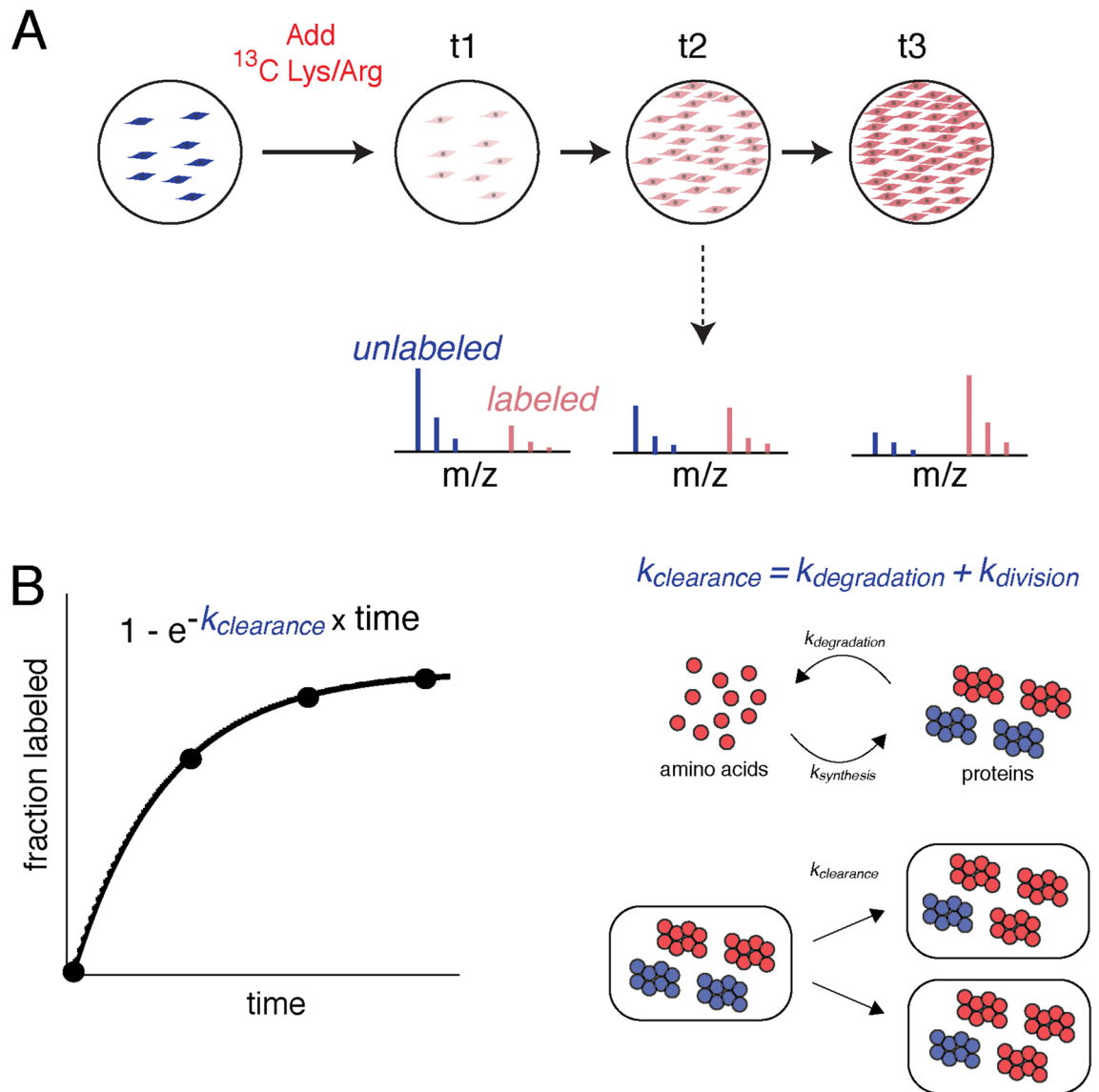
Figure 1. Design and quantitative analysis of dynamic stable isotopic labeling of amino acids in cell culture (dSILAC) experiments. (**A**) Experimental design. Cultured cells are grown in the presence of ^{13}C-lysine and ^{13}C-arginine. Newly synthesized proteins incorporate these heavy-labeled amino acids as the original pool of unlabeled proteins is cleared over time. The kinetics of fractional labeling of proteins is measured by LC–MS/MS using a bottom-up proteomics workflow. (**B**) Quantitative analysis. The first order rate constant of fractional labeling is a measure of the protein clearance rate. Two factors contribute to the rate of clearance: the rate of dilution due to cell division and the rate of protein degradation. The blue and red colors respectively represent unlabeled and labeled amino acids, proteins, spectra and cells.

cells is substantially slowed upon formation of PrP^{Sc} aggregates and validates dSILAC as a methodology capable of quantitatively analyzing changes protein clearance kinetics in N2a-Cl3 cells.

Global effect of PrP^{Sc} accumulation on proteome turnover. The data obtained from the dSILAC experiment described in Fig. 2B were used to analyze the proteome-wide effect of PrP^{Sc} aggregates on protein clearance (Supplementary Tables S1–S3). We limited our analysis to 4,730 proteins where heavy to light ratios (H/L) could be quantified for two or more peptides in at least three timepoints in both −QA and +QA samples (Table 1). In order to determine the true degradation rates ($k_{degradation}$) of proteins, the rate of cell division was subtracted from the measured rate of clearance ($k_{clearance}$). Figures 3A–C provide a comparison of protein $k_{degradation}$ values between −QA and +QA cells as histograms, pairwise scatter plot and log$_2$ ratios. Globally, it is evident that unlike PrP itself, prion infection does not result in dramatic reductions in degradation rates of most proteins in N2a-Cl3 cells. Indeed, we observed a slight but statistically significant proteome-wide increase in
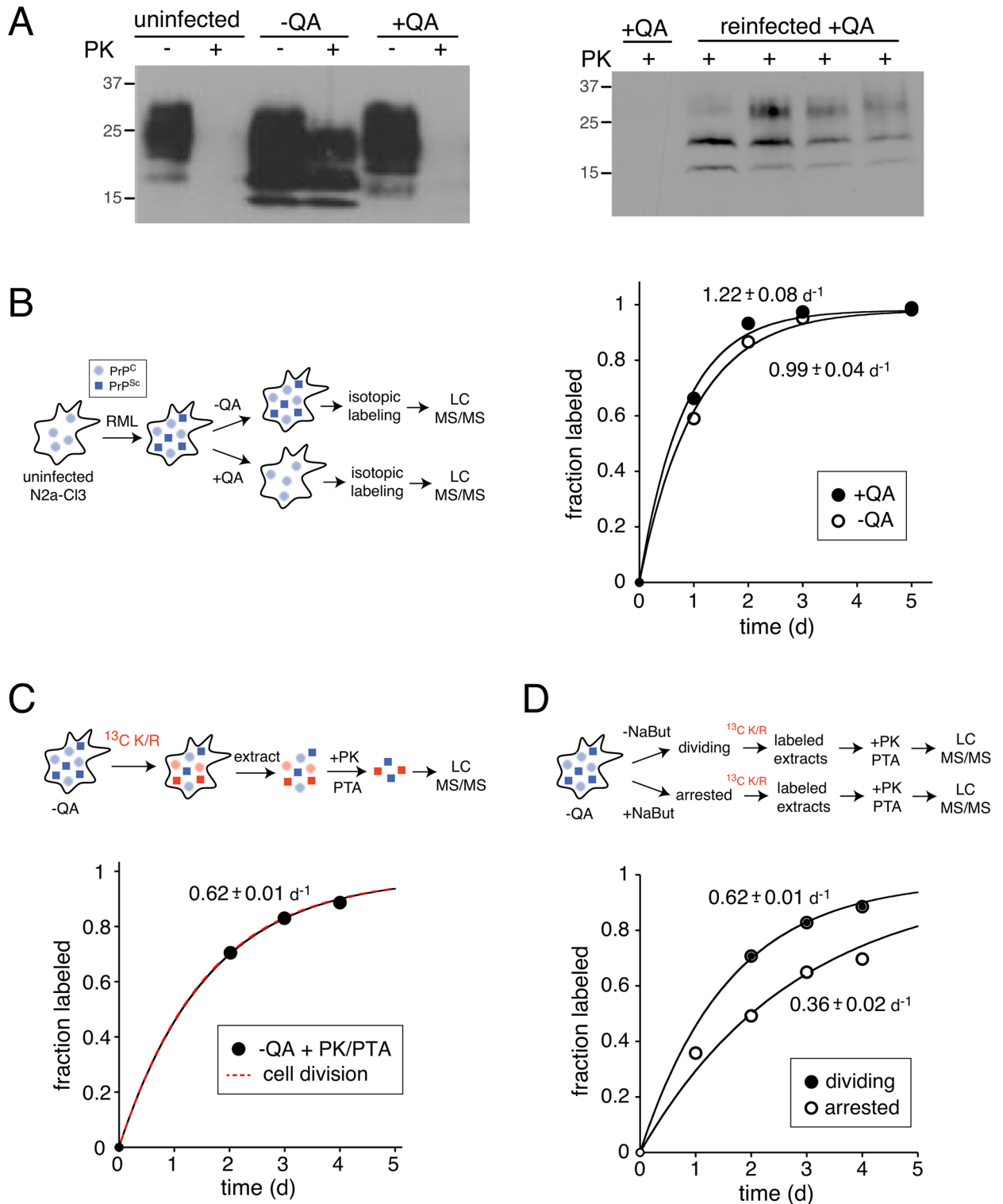
Figure 2. The clearance kinetics of PrP^C and PrP^{Sc}. (**A**) Prion infected and uninfected cell models. N2a-Cl3 cells were infected with the RML prion strain (−QA). Some cultures were passaged in the presence of quinacrine to generate an uninfected control (+QA). The presence and absence of protease-resistant PrP^{Sc} in −QA and +QA samples were verified by western blots following proteinase K (PK) digestion (left). To establish that +QA cells can be reinfected with prions, they were split into five populations and four of these were exposed to lysates from a −QA culture. After five passages, protease-resistant PrP^{Sc} was detectable in the four re-infected +QA cultures by western blots following PK digestion (right). (**B**) Clearance kinetics of total PrP. −QA and +QA cultures were propagated in labeling media containing ^{13}C Lysine/Arginine, harvested at different time points and analyzed by LC–MS/MS as described in Fig. 1. The kinetic plots indicate the average fractional labeling of all peptides mapped to PrP (PrP^C for +QA and PrP^C plus PrP^{Sc} for −QA). (**C**) Clearance kinetics of PrP^{Sc}. Lysates from −QA cells were subjected to PK digestion to isolate protease resistant PrP^{Sc} prior to LC–MS/MS

analysis. Clearance kinetics were analyzed as in (**B**). (**D**) The effect of cell division on the clearance rate of PrP^{Sc}. To determine the contribution of cell division to PrP^{Sc} clearance, a population of −QA cells was treated with sodium butyrate to halt cell division prior to dSILAC analysis. Clearance kinetics were analyzed as in (**B**). The results indicate that PrP^{Sc} aggregates are cleared more rapidly in dividing cells.

Cells	Peptides identified	Proteins identified	Peptides quantified	Proteins quantified	Median k_{deg} (day^{-1})	Shared proteins
−QA	64,648	7,280	58,590	5,215	0.27	4,730
+QA	63,355	7,196	59,320	5,168	0.24	

Table 1. Coverage of dSILAC experiments.

degradation rates in −QA cells (Fig. 3B, C). In order to confirm this observation using an orthogonal biochemical approach, we conducted a pulse-chase analysis using ʟ-Azidohomoalanine (AHA), an analog of methionine that can be incorporated into newly synthesized proteins, coupled to biotin by copper-mediated click chemistry and visualized using avidin-based fluorescence detection[46,47]. Using this approach, we were able to confirm that the overall rate of protein turnover is moderately increased in prion infected cells (Fig. 3D).

The proteome-wide data supports the hypothesis that the accumulation of prion aggregates results in the upregulation of cellular degradation machinery. Interestingly, we observed that the increase in degradation rates is disproportionately evident in long-lived proteins, defined as proteins with $k_{degradation}$ values less than 0.2 day^{-1} (Fig. 4A). In eukaryotic cells, the two main protein degradation pathways with general selectivity are the UPS and lysosomal pathways, such as autophagy. It is generally accepted that short-lived proteins are primarily degraded by the UPS, whereas long-lived proteins are primarily degraded by the lysosome[31,48]. We therefore explored the possibility that prion infection results in the upregulation of the autophagy pathway, resulting in an increase in the degradation rate of autophagic substrates.

In a previous study, we conducted a proteome-wide dSILAC study to identify proteins whose degradation rates are diminished in cells lacking two core components of canonical autophagy: Atg5 and Atg7[32]. The study identified the subunits of the 26S proteasome and the CCT/TRiC chaperonin as substrates of basal autophagy. As a counter-example, the degradation rate of the ribosome was unaltered in Atg5 and Atg7 knockout backgrounds, indicating that it was excluded from basal autophagy. We determined how the degradation rates of these complexes are impacted by prion infection (Fig. 4B). Our data indicate that the degradation of the proteasome and CCT/TRiC are increased in −QA cells in comparison to +QA cells. Conversely, the degradation rate of ribosomal subunits remained unchanged. To confirm the altered degradation of a basal autophagy substrate using an alternative approach, we conducted a pulse-chase AHA labeling experiment (as in Fig. 3D) and probed for the proteasomal subunit PSMB1 after streptavidin purification of AHA-labeled proteins (Fig. 4C). The results corroborated our proteomic approach and are consistent with the idea that the rate of autophagy is enhanced in prion infected cells.

Enhancement of autophagy in prion infected cells. Using western blots, we analyzed −QA and +QA extracts for a number of reporters associated with autophagy and lysosomal degradation (Fig. 5A). These included Cathepsins D, L and A (lysosomal hydrolases), LC3-II (marker of autophagsomes) and p62/SQSTM1 (autophagy substrate and reporter of autophagic flux)[49,50]. We observed an increase in the level of LC3-II relative to LC3-I, indicating an increase in the steady-state levels of autophagosomes in prion infected cells. Consistent with the upregulation of autophagic flux, our dSILAC results indicate that p62/SQSTM1 degradation rates are increased in prion infected cells (Fig. 5B). Interestingly, despite its enhanced degradation, the steady-state levels of p62/SQSTM1 are not drastically diminished in prion infected cells (Fig. 5A). This observation is consistent with previous reports showing that N2a cells exhibit increased expression of p62/SQSTM1 mRNA upon prion infection[18]. Additionally, we observed that levels of some, but not all, lysosomal cathepsins are greatly enhanced in prion infected cells (Fig. 5A). This effect was particularly dramatic for cathepsin D. To verify this finding, total cathepsin D enzymatic activity was assayed in −QA and +QA using a synthetic fluorescent substrate. The data indicated that the total activity of cathepsin D is significantly increased in prion infected cells (Fig. 5C). To determine whether this increase in activity may be due to overall expansion of lysosomal compartments, the total lysosomal volume within −QA and +QA cells were quantified using a fluorometric lysosomal stain (CytoPainter). The data indicated that there is a significant expansion of total lysosomal volume in prion infected cells (Fig. 5D). Together, the data suggest that prion infection is associated with the upregulation of specific molecular components of lysosomal degradation. Specifically, prion infection in N2a cells is associated with expansion of lysosomal compartments and enhanced delivery of protein targets to lysosomes resulting from the activation of the autophagy pathway.

Discussion

The cytopathology of prion disease is known to be intimately linked to the lysosomal degradation system. Expansion of lysosomes, late endosomes, and autophagic vesicles are well-established neuropathological features of prion infected cells both in vivo and in vitro[10,51,52]. Delivery of PrP^{Sc} to lysosomes by autophagy is a key pathway for its degradation, and levels of intracellular PrP^{Sc} are readily modulated by inhibition or activation
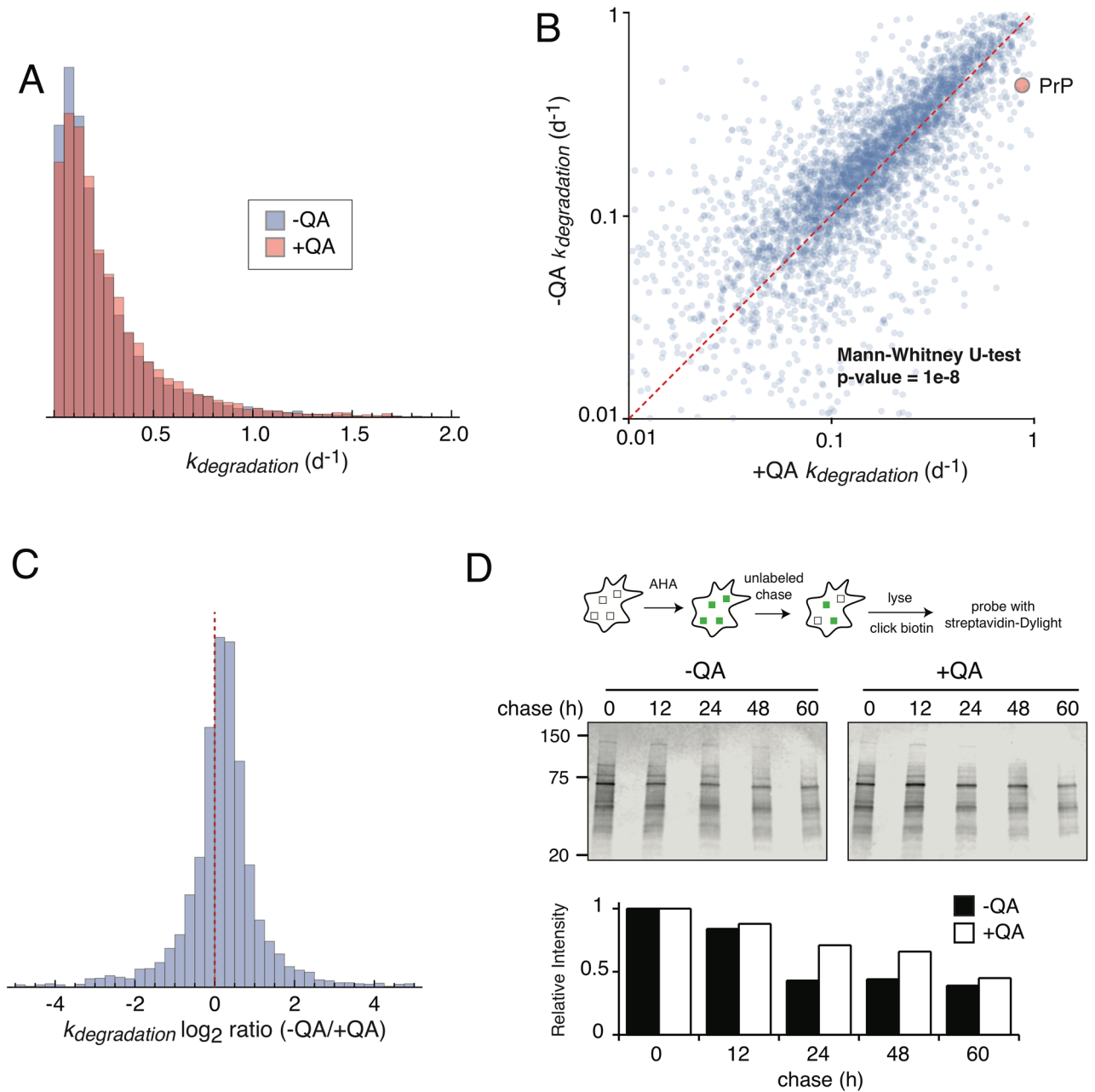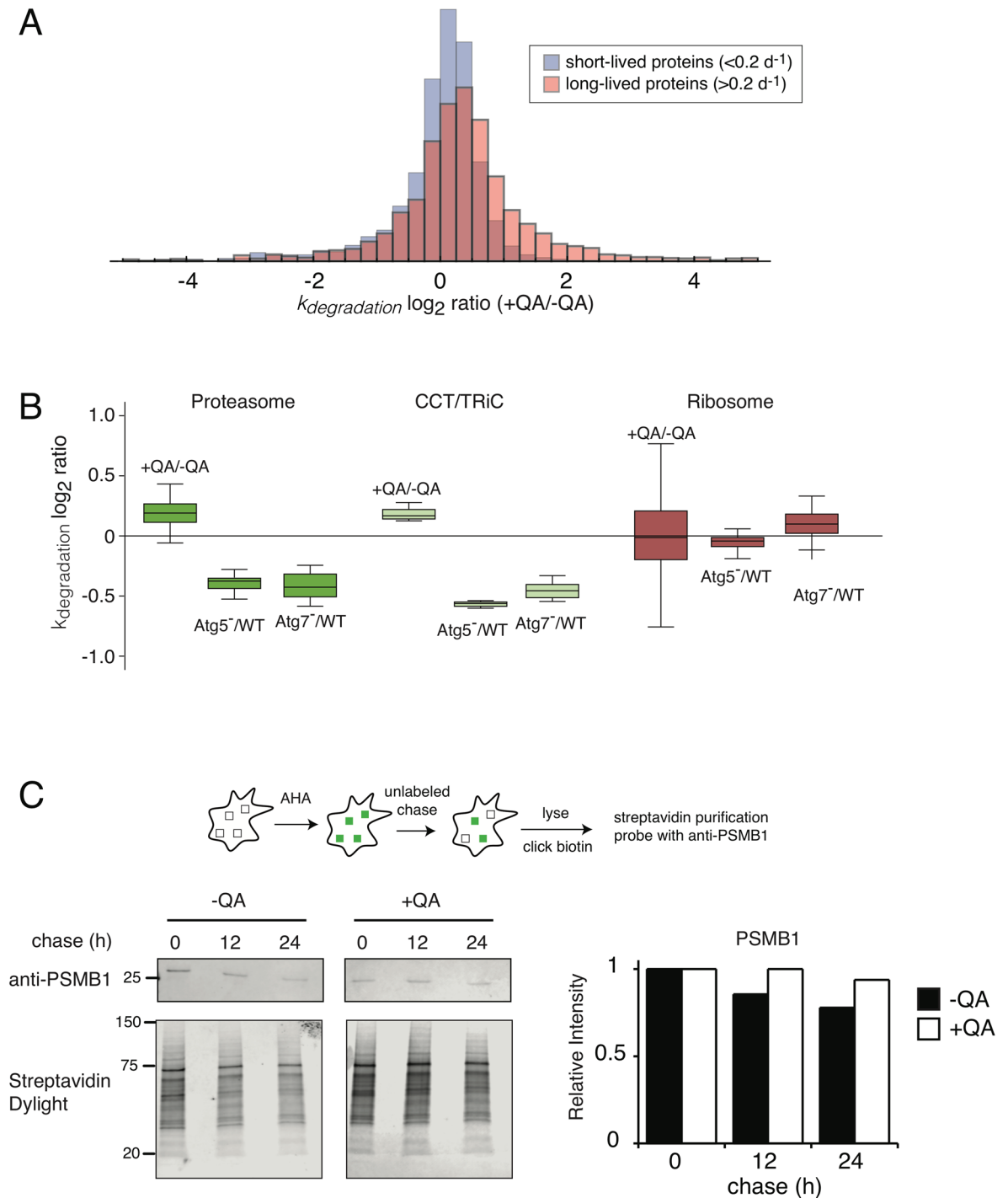
Figure 3. Global analysis of protein degradation rates. Using dSILAC, degradation rates were measured for 4,730 proteins shared between −QA and +QA samples. The rates are compared as distribution plots (**A**), pairwise comparisons (**B**) and log₂ ratios (**C**). In (**B**), the dotted line indicates the identity line and red circle indicates the comparison of PrP^C and PrP^Sc in −QA and −QA samples, respectively. The −QA and +QA datasets differ with a p-value of 1e-8 using the Mann Whitney U-test. (**D**) Analysis of proteome degradation kinetics by ʟ-Azidohomoalanine (AHA) labeling. Cultures of −QA and +QA cells were labeled with AHA for 16 h and chased with unlabeled media for variable lengths of time. Labeled proteins were biotinylated by copper-mediated click chemistry and detected by western blots. Relative intensities of labeled proteins were quantified as described in "Methods".

of autophagy[53,54]. During prion infection, the conversion of PrP^C to PrP^Sc results in its intracellular stabilization where it accumulates in late endosomes and lysosomes[7,11]. The accumulation of PrP^Sc aggregates in lysosomal compartments has the potential to influence lysosomal degradative pathways that are normally responsible for turnover of a significant fraction of the cellular proteome. Accordingly, a number of studies have sought to characterize the impact of prion infection on protein degradation and cellular proteostasis. In a recent study, Homma et al. showed that prion infection impairs the degradative capacity of lysosomes by interfering with their maturation[18]. Other studies have shown that autophagy is upregulated in prion infected tissues and cells, suggestive of a possible compensatory response to restore proteostasis upon accumulation of PrP^Sc[10,51,52]. However, in these studies, changes in protein degradation were monitored for a small number of markers and individual
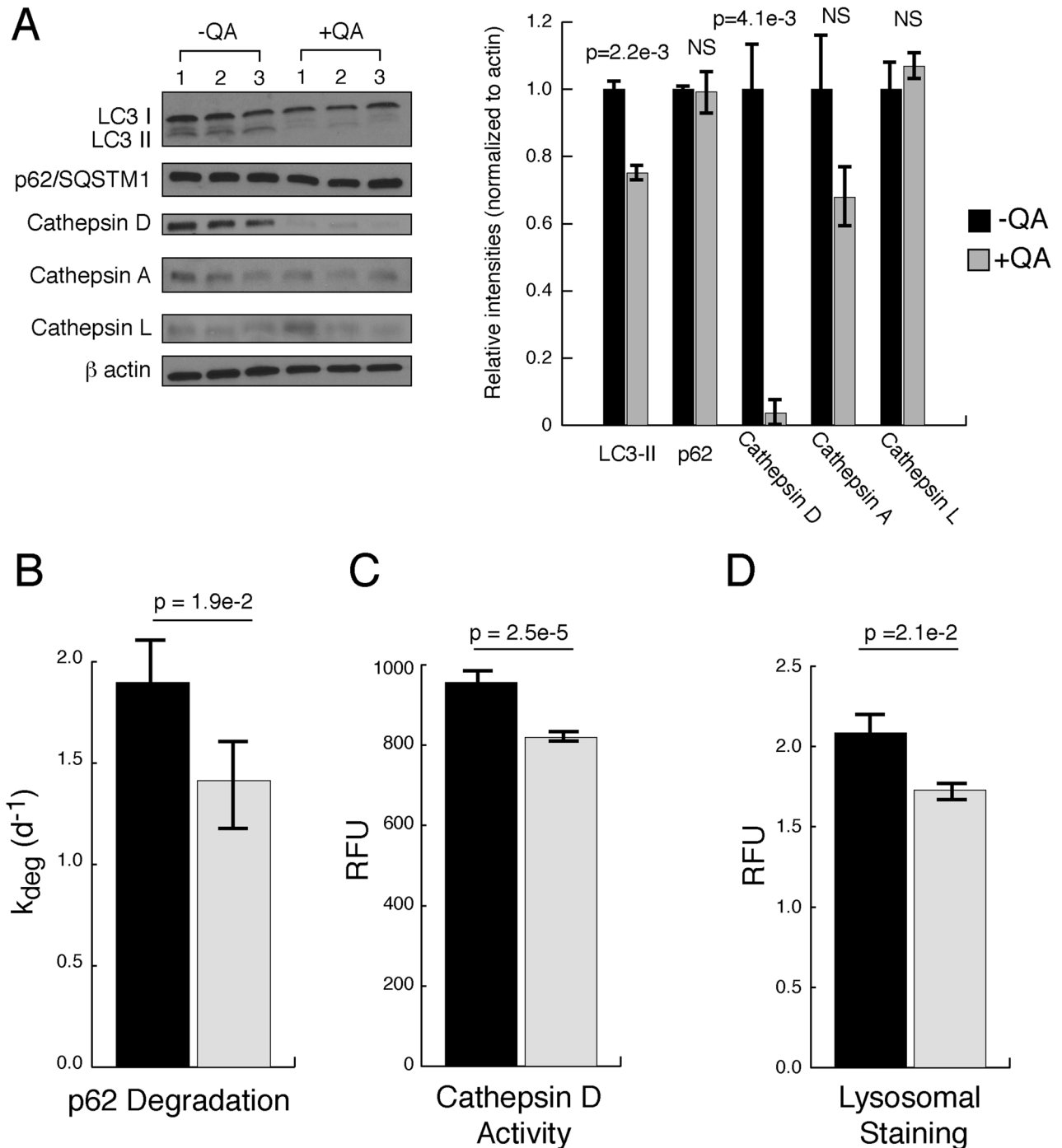
Figure 4. The degradation rates of long-lived proteins and autophagy substrates are increased in prion infected cells. (**A**) The $\log_2$ ratio of degradation rates between −QA and +QA samples for short-lived ($k_{degradation} > 0.2$ day^{-1}) and long-lived ($k_{degradation} < 0.2$ day^{-1}) proteins. (**B**) The effect of prion infection on $k_{degradation}$ of two previously established substrates of basal autophagy (the proteasome and CCT/TRiC) and the ribosome, previously shown to be excluded from basal autophagy by Zhang et al. The change in degradation rates in autophagy-deficient cells (ATG5$^{-/-}$ and ATG7$^{-/-}$) compared to wildtype, measured by Zhang et al., is shown for comparison. (**C**) Analysis of PSMB1 degradation kinetics by AHA labeling. Cultures of −QA and +QA cells were labeled with AHA for 16 h and chased with unlabeled media for variable lengths of time. Labeled proteins were biotinylated by copper-mediated click chemistry and subsequently purified from total cell lysates using Streptavidin magnetic beads. Purified PSMB1 was detected through western blot analysis and compared to total purified protein. Relative intensities of labeled proteins were quantified as described in "Methods".

Figure 5. Biochemical analysis of markers of lysosomal degradation. (**A**) Western blot analysis of −QA and +QA protein lysates (done in biological triplicate) indicate significant increases in LC3-II and cathepsin D abundance in −QA cells, whereas little change is observed in levels of Cathepsins A, L and p62/SQSTM1. Similarly, the abundance of the major lysosomal hydrolase cathepsin D is significantly increased in −QA cells. (**B**) While the abundance p62/SQSTM1 is not significantly altered during prion infection (**A**), the degradation rate of p62/SQSTM1 (determined by dSILAC analysis) is increased. Error bars were generated by calculating the standard error of the mean for the degradation rates of individual peptides used in determining the degradation rate of p62/SQSTM1 (n = 6). (**C**) Consistent with increases in its steady-state levels (**A**), the total enzymatic activity of Cathepsin D is increased in prion infected −QA cells (n = 6). (**D**) Total lysosomal volume, determined by a fluorometric lysosomal stain, is increased in prion infected −QA cells (n = 8). The error bars indicate standard error of the mean. Comparisons between −QA and +QA samples were conducted by two-tailed Student t-test. Numbers above the bar graphs indicate the calculated p-value.

proteins, making it difficult to assess the proteome-wide effects of prion infection on protein degradation. To overcome this limitation, we used a dSILAC strategy to quantify changes in proteome degradative flux in prion infected cells. Our results provided a number of insights regarding the effects of prion infection on the degradation kinetics of PrP and the proteome at large.

Consistent with previous studies, our results indicate that the degradation rate of protease-resistant PrP^{Sc} in N2a-Cl3 cells is significantly slower than PrP^C. Our measured degradation rates for PrP^C and protease-resistant PrP^{Sc} were 0.70 day^{-1} (half life = 1.0 days) and 0.40 day^{-1} (half life = 1.7 days), respectively. The measured degradation rate for protease-resistant PrP^{Sc} is consistent with rates previously measured in a bigenic mouse model (half-life = 1.5 days)[55] and ScN2a cells measured by radiolabeled pulse-chase experiments (half-life > 1 days)[8]. The measured degradation rate for PrP^C, although comparable to that reported for bigenic mice (half life = 18 h)[55], is slower than that previously reported for N2a cells (half life = 5 h)[8]. A number of factors may account for this discrepancy. First, in this study, we have used a transgenic overexpression variant of N2a cells. The increased expression level of PrP may influence its clearance kinetics by formation of non-infectious aggregates, as has been previously reported for some mouse overexpression lines[56] or through partial inhibition of protein degradation pathways. Alternatively, this discrepancy may be due to differences in the methodology used for measurement of degradation rates. In previously conducted pulse-chase analyses, newly synthesized proteins were labeled with short pulses of ^{35}S-methionine and their degradation kinetics were measured following an unlabeled chase[8]. Here, our methodology involved continuous labeling experiments where the turnover of the entire protein pool (not just newly synthesized proteins) was monitored over time. It has recently been shown that the turnover of many proteins is multiphasic, and a large fraction of newly synthesized proteins are rapidly degraded before becoming incorporated into the steady-state protein pool[57]. Thus, short-term pulse-chase experiments may underestimate the half-life of the steady-state protein pool. Consistent with this idea, our measured PrP^C half-life closely matches values measured in cultured mouse neurons by long-term stable isotope labeling experiments[33]. Regardless, the relative stabilization of protease-resistant PrP^{Sc} that was reported in previous studies was recapitulated in our experiments.

Importantly, our results indicate that, in prion infected cells, protease-resistant PrP^{Sc} is sufficiently stabilized such that its dominant route of clearance in dividing ScN2a cells is cellular dilution through cytokinesis rather than proteolytic degradation. These results are consistent with previous results showing that PrP^{Sc} levels increase in cultured cells when they reach a state of confluency and there is a reduction in the division rate[58]. In this way, the clearance of protease-resistant PrP^{Sc} in dividing cultured cells fundamentally differs from postmitotic neurons in vivo, where the catabolism of PrP^{Sc} is the sole route of clearance.

Our data indicate that the impact of prion infection on global protein degradation is generally subtle. The median prion-induced change in the degradation rate of the proteome is ~ 10% (Fig. 3, Table 1). Nonetheless, there is a statistically significant enhancement of degradation rates for long-lived proteins, including at least two protein complexes (the proteasome and CCT/TRiC chaperonin) that were previously shown to be substrates of basal autophagy[32]. Conversely, the degradation of short-lived proteins known to be enriched in substrates of UPS[31], and the ribosome which was shown to be excluded from basal autophagy[32], are minimally impacted by prion infection. Consistent with previous studies[16,18], we further showed that levels of LC3-II, a marker of autophagosomes, and expression levels of specific lysosomal hydrolases are increased in prion infected cells. This upregulation was accompanied by an overall expansion of lysosomal compartments in the cell. Together, the data provide evidence that that the rate of autophagic flux is enhanced in N2a cells in response to prion infection.

Our results highlight two potential mechanisms that may enable dividing N2a cells to maintain viability in a prion infected state. First, the process of cell division acts as a continuous clearance mechanism, reducing the steady-state level of PrP^{Sc} in dividing cells. Second, the activation of autophagy may partially mitigate the proteostatic disruptions caused by the formation and accumulation of PrP^{Sc}. By enhancing the rate of autophagic flux, the cells stimulate a degradation system that may counter the stability of PrP^{Sc} and enhance the turnover of other autophagic substrates. The generality of these findings to cell types other than N2a remains to be determined. Nonetheless, as has been shown in a number of in vivo and in vitro experiments[13], our results suggest that further enhancement of autophagy through pharmacological induction of lysosomal activity may provide a promising strategy for clearance of PrP^{Sc} and maintaining proteostasis in prion infected cells.

Methods

Cell culture. N2a-Cl3 cells previously infected with the Rocky Mountain Laboratories strain of prion aggregate (RML) were generously provided by the Prusiner laboratory[37,38]. Cultures were maintained in Eagle's Minimum Essential Medium (ATCC) supplemented with 15% FBS (Invitrogen), 100 U/mL penicillin, 100 U/mL streptomycin at 37 °C with 5% CO$_2$. To create uninfected controls, prion infected cells were treated with 4 μM of quinacrine and cleared of prion infection within four passages.

Stable isotope labeling. The isotopic labeling procedure was similar to that previously described by Zhang et al.[35] The media utilized for isotopic labeling was Eagle's Minimum Essential Medium (ATCC) supplemented with 15% dialyzed FBS (Thermo Scientific), 100 U/mL penicillin, and 100 U/mL streptomycin. Cells were gradually adapted to this media by replacing normal FBS with dialyzed FBS within five passages. Cells were then plated at a density of 1,000,000 cells per 10-cm plate.

One day after plating, the dividing cultures were switched to MEM labeling media for SILAC (Thermo Scientific) supplemented with L-arginine:HCl (^{13}C6, 99%) and L-lysine:2HCl (^{13}C6, 99%; Cambridge Isotope Laboratories) at concentrations of 0.1264 g/L and 0.087 g/L, 15% dialyzed FBS (Thermo Scientific), 100 U/mL penicillin, and 100 U/mL streptomycin. For whole proteome analysis, cells were collected after 0, 1, 2, 3, and

5 days of labeling and washed with PBS. For analysis of isolated PrP^{Sc} aggregates, cells were collected after 0, 1, 2, 3, and 4 days of labeling and washed with PBS. All cell pellets were frozen before further analysis.

Mass spectrometry sample preparation.   The MS sample preparation procedure was similar to that previously described by Swovick et al. [35] Cells were lysed with ice-cold lysis buffer (10 mM Tris·HCl pH 8.0, 0.15 M NaCl, 0.5% Nonidet P-40, 0.48% SDS). Cell lysates were centrifuged at 16,000×g for 10 min and the supernatants were then transferred to new Eppendorf tubes. Protein concentrations were measured by the bicinchoninic assay (BCA) kit (Thermo Scientific).

When processing lysates for prion protein peptides, 20 μg of proteinase K (fungal) (Thermo Scientific) was added to 1 mg cell lysates in 1 mL of lysis buffer. Lysates were incubated for 1 h at 37 °C. 20 μL of PMSF was added to lysates for a final concentration of 20 mM. Sodium lauroyl sarcosinate was added for a final 1% weight-to-volume concentration, and 75 μL of Phosphotungstic acid (pH 7.4) was added for a final 0.75% weight-to-volume to precipitate aggregated proteins from the lysate. Lysates were incubated for 3 h at 37 °C while shaking at 350 rpm. Lysates were then centrifuged at 16,000×g for 30 min and the supernatants were then transferred to new Eppendorf tubes, leaving 30 μL of buffer to resuspend pelleted aggregates. 12.5 μL of resuspended pellets were added to 12.5 μL of 5% SDS and boiled for 5 min before further processing.

Protein lysates after proteinase K digestion, as well as 25 μg of total protein from whole cell extracts, were processed into peptides by the following S-trap protocol (Protifi). Reduction of disulfide bonds was performed with 5 mM Tris(2-carboxyethyl)phosphine (TCEP) Bond-breaker (Thermo Scientific) at RT for 1 h, and protein alkylation was performed with 10 mM iodoacetamide (IAA) at RT for 30 min in darkness. DTT was added to 1 mM to quench IAA and samples were applied to S-Trap Micro Spin Columns (Protifi). To derive tryptic peptides, 20 μL of 50 ng/μL trypsin (selective cleavage on the C-terminal side of lysine and arginine residues) was added and the samples were incubated overnight at 37 °C in a water bath. Peptides were released from the column using subsequent washes of 0.1% TFA followed by 50% ACN in 0.1% TFA.

To increase proteome coverage, high-pH fractionation was conducted on whole cell extracts before LC–MS/MS using homemade C18 spin columns. Samples were dried down and resuspended in 50 μL of 100 mM ammonium formate (pH 10). Eight different elution buffers were made in 100 mM ammonium formate (pH 10) with 5%, 7.5%, 10%, 12.5%, 15%, 17.5%, 20%, and 50% acetonitrile added. After conditioning the column with acetonitrile and 100 mM ammonium formate, the samples were added and centrifuged. An ammonium formate wash was performed to remove any residual salt before the eight elutions were collected in fresh tubes. All samples were then dried down and re-suspended in 15 μL of 0.1% TFA.

LC–MS/MS analysis.   The proteome-wide analysis of protein degradation (illustrated in Fig. 2B) was conducted on a Q Exactive Plus LC–MS/MS instrument and analysis of isolated PrP^{Sc} (illustrated in Fig. 2C and D) was conducted a Fusion Lumos LC–MS/MS instrument. The MS methods were similar to those previously described[59,60] and are briefly outlined below.

Q Exactive Plus LC–MS/MS.   Peptides were injected onto a homemade 30 cm C18 column with 1.8 um beads (Sepax), with an Easy nLC-1000 HPLC (Thermo Fisher), connected to a Q Exactive Plus mass spectrometer (Thermo Fisher). Solvent A was 0.1% formic acid in water, while solvent B was 0.1% formic acid in acetonitrile. Ions were introduced to the mass spectrometer using a Nanospray Flex source operating at 2 kV. Optimized gradients for individual fractions were employed, as shown in Supplementary Table S4. The Q Exactive Plus was operated in data-dependent mode, with a full scan followed by 20 MS/MS scans. The full scan was done over a range of 400–1,400 m/z, with a resolution of 70,000 at m/z of 200, an AGC target of 1e6, and a maximum injection time of 50 ms. Peptides with a charge state between 2 and 5 were picked for fragmentation. Precursor ions were fragmented by higher-energy collisional dissociation (HCD) using a collision energy of 27 and an isolation width of 1.5 m/z, with an offset of 0.3 m/z. MS2 scans were collected with a resolution of 17,500, a maximum injection time of 55 ms, and an AGC setting of 5e4. Dynamic exclusion was set to 25 s.

Fusion Lumos LC–MS/MS.   The HPLC and ion source set-up was identical to the Q Exactive, except that the nLC was a 1,200 series with 80% acetonitrile in 0.1% formic acid as solvent B. The gradient began at 3% B and held for 2 min, increased to 10% B over 5 min, increased to 38% B over 38 min, then ramped up to 90% B in 3 min and was held for 3 min, before returning to starting conditions in 2 min and re-equilibrating for 7 min, for a total run time of 60 min. The Fusion Lumos was operated in data-dependent mode, while also employing an inclusion list containing SILAC labeled PrP peptides that was created using the Skyline software program (Supplementary Table S5). An MS2 scan would be triggered when a precursor ion was within 10 ppm of a m/z value on the inclusion list. Otherwise, the method proceeded as usual. The cycle time was set to 1.5 s. Monoisotopic Precursor Selection (MIPS) was set to Peptide. The full scan was done over a range of 375–1,400 m/z, with a resolution of 120,000 at m/z of 200, an AGC target of 4e5, and a maximum injection time of 50 ms. Peptides with a charge state between 2–5 were picked for fragmentation. Precursor ions from the inclusion list and those selected by the data-dependent method were fragmented by collision induced dissociation (CID) using a collision energy of 30% and an isolation width of 1.1 m/z. MS2 scans were collected with the ion trap scan rate set to rapid, a maximum injection time of 200 ms, and an AGC setting of 1e4. Dynamic exclusion was set to 20 s.

Data analysis and kinetic models.   dSILAC data analysis was conducted essentially as previously described by Swovick et al.[36]. MS2 data for all samples were searched against the *M. musculus* (22,305 entries, downloaded 8/7/2017) uniprot databases using the integrated Andromeda search engine with MaxQuant soft-

ware. Peptide searches were done as previously described[36] with the addition of the match-between-runs with a match time window of 0.7 min and an alignment time window of 20 min (Supplementary Table S6).

The determination of degradation rate constants ($k_{degradation}$) from fraction labeled measurements were conducted in accordance to the kinetic model outlined previously[36].

Western blotting. Cells were lysed with ice-cold lysis buffer (10 mM Tris·HCl pH 8.0, 0.15 M NaCl, 0.5% Nonidet P-40, 0.48% SDS). Cell lysates were centrifuged at 16,000×g for 10 min and the supernatants were then transferred to new Eppendorf tubes. For Western blot analysis, 20 μg was separated by electrophoresis in 10% polyacrylamide gels and transferred to polyvinylidene difluoride membranes using Trans-Blot Turbo Transfer System (Biorad). After 1 h of incubation at room temperature in Odyssey Blocking Buffer in TBS (Licor), the membrane was incubated with the indicated antibodies at 4 °C overnight. The membranes were then washed with TBST/0.1% Tween 20, and the corresponding secondary antibodies were applied to the membranes for 1 h at room temperature. The membranes were then washed with TBST/0.1% Tween 20, and the detection of signal was done using an enhanced chemiluminescence detection kit (Pierce). The primary antibodies and the corresponding dilutions utilized for the Western blots were Anti beta-Actin Antibody: 1:5,000 (Abcam); Anti-p62 (SQSTM1) Antibody: 1:1,000 (MBL International); Anti-LC3 Antibody: 1:1,000 (MBL International); Cathepsin A (A-19): 1:1,000 (Santa Cruz Technology), Cathepsin D (c-20): 1:1,000 (Santa Cruz Technology), Cathepsin L: 1:1,000 (Santa Cruz Technology), and anti-PrP (D18) 1:1,000 (provided by the Pruisner laboratory). In instances where multiple proteins of varying molecular weights were analyzed from the same SDS/PAGE gel, the membrane was cut into multiple parts following transfer. Each part was probed with a different primary antibody against a specific target protein and, subsequently, with the corresponding secondary antibody.

Cathepsin activity analysis. Cathepsin D activity (used as a proxy for total lysosomal hydrolase activity) was measured by using Cathepsin D Activity Assay Kit (Abcam) as previously described[35]. Cells were collected, and 350 μL of lysis buffer was used to lyse 1 million cells; 5 μL of lysate was incubated in substrate/buffer solution for 75 min at 37 °C. Enzyme activity was measured by monitoring release of the fluorescent cleavage product, MCA. Activity measurements from parallel reactions containing 0.7 μM protease inhibitor pepstatin A were subtracted from the activity measurements obtained without the inhibitor. Fluorescence was quantified by SpectraMax M5 at Ex/Em = 328/460 nm.

Lysosomal quantification. Lysosomal quantity was measured using the Lysosomal Staining Kit—Green Fluorescence—Cytopainter (Abcam) as previously described[35]. Cells were plated at 60,000 cells per well of a 96 well plate. One day after plating, media was replaced with the dye working solution and incubated for 60 min at 37 °C. Parallel reactions containing 10 nM of the lysosomal inhibitor Bafilomycin were used to measure background fluorescence. Fluorescence was quantified by SpectraMax M5 at Ex/Em = 490/525 nm.

Prion aggregate reinfection of quinacrine cleared cells. N2a-Cl3 RML cells treated with 4 μM of quinacrine and shown to be cleared of prion infection were split into five populations. Four of these populations were incubated for 6 h with 20 mg of protein lysate obtained from N2a-Cl3 RML cells lysed through freeze–thaw lysis in hypotonic buffer (0.1 mM PMSF, 1 mM DTT, 0.2% NP-40). All five populations were maintained for five passages then assayed for protease-resistant prion infection using aforementioned proteinase K digestion methods and western blot analysis.

ʟ-Azidohomoalanine pulse-chase labeling. One day after plating, dividing N2a-Cl3 cultures were switched to RPMI 1640 medium supplemented with 10% FBS (Thermo Scientific), 100 U/mL penicillin, and 100 U/mL streptomycin for 24 h. These RPMI-adapted cultures were then incubated with RPMI medium without methionine and supplemented with 10% FBS, 100 U/mL penicillin, 100 U/mL streptomycin, and 83 μM ʟ-Azidohomoalanine for 16 h. Cultures were then switched to chase medium RPMI 1640 supplemented with 10% FBS 100 U/mL penicillin and 100 U/mL streptomycin. Cells were collected 0, 12, 24, 48, and 60 h after switching to chase media and washed with PBS. All cell pellets were frozen before further analysis.

Analysis of total protein turnover by AHA pulse-chase experiment. Cells obtained after ʟ-Azidohomoalanine labeling were lysed through freeze–thaw lysis in hypotonic lysis buffer. 200 μg of total protein from each lysate were coupled to biotin by copper-mediated click chemistry (Invitrogen) and 40 μM of biotin alkyne. Chase timepoints were loaded onto 10% polyacrylamide gels in increasing quantities consistent with the growth rate of cells found during the RPMI chase (growth rates for -QA and +QA cell were measured as 0.013 d^{-1} and 0.0094 d^{-1}, respectively). Proteins were then separated by electrophoresis and transferred to polyvinylidene difluoride membranes using Trans-Blot Turbo Transfer System (Bio-Rad). Membranes were incubated for 1 h using Odyssey Blocking Buffer in TBS (Licor) and then incubated at room temperature with Streptavidin protein, DyLight 800 conjugated: 1:1000 (Thermo). The membranes were then washed with TBST/0.1% Tween 20, and signal was detected using the Licor Odyssey CLx and Image Studio v5.2. Signal intensity for each timepoint was calculated by plotting the median relative fluorescent intensity found in 8 identical segments along the length of each lane.

Analysis of PSMB1 turnover by AHA pulse-chase experiment. Cells obtained after ʟ-Azidohomoalanine labeling were lysed through freeze-thaw lysis in hypotonic lysis buffer. 40 μg of total protein from each lysate were coupled to biotin by copper-mediated click chemistry (Invitrogen) and 40 μM of Biotin alkyne. Free

biotin was then purified from the reactions using PD SpinTrap G-25 columns (Life Sciences) equilibrated with phosphate-buffered saline. These purified samples were then incubated overnight with Streptavidin magnetic beads (Pierce). The beads were washed three times using 0.1% Tween in PBS and proteins were eluted off the beads by boiling in Laemmli sample buffer (Bio-Rad).

Western blot analysis on 20 µg from each elution off the Streptavidin magnetic beads was done in accordance to aforementioned western blotting techniques utilizing the following antibodies and corresponding dilutions – 20S Proteosome β1 (FL-241): 1:1,000 (Santa Cruz) with Goat anti-rabbit IgG secondary antibody, DyLight 800 conjugate**:** 1:10,000 (Thermo) and Streptavidin protein, DyLight 800 conjugated: 1:1,000 (Thermo). Blots were visualized and signal intensities were measured using the Licor Odyssey CLx and Image Studio v5.2.

Data availability

References

1. Prusiner, S. B. Molecular-biology of prion diseases. *Science* **252**, 1515–1522 (1991).
2. Colby, D. W. & Prusiner, S. B. Prions. *Cold Spring Harb. Perspect. Biol.* **3**, a006833 (2011).
3. Collinge, J. Mammalian prions and their wider relevance in neurodegenerative diseases. *Nature* **539**, 217–226 (2016).
4. Aguzzi, A. & Weissmann, C. Prion diseases. *Haemophilia* **4**, 619–627 (1998).
5. Watts, J. C., Balachandran, A. & Westaway, D. The expanding universe of prion diseases. *PLoS Pathog.* **2**, e26 (2006).
6. Goold, R. *et al.* Rapid cell-surface prion protein conversion revealed using a novel cell system. *Nat. Commun.* **2**, 281 (2011).
7. Borchelt, D. R., Taraboulos, A. & Prusiner, S. B. Evidence for synthesis of scrapie prion proteins in the endocytic pathway. *J. Biol. Chem.* **267**, 16188–16199 (1992).
8. Borchelt, D. R., Scott, M., Taraboulos, A., Stahl, N. & Prusiner, S. B. Scrapie and cellular prion proteins differ in their kinetics of synthesis and topology in cultured cells. *J. Cell Biol.* **110**, 743–752 (1990).
9. Fehlinger, A. *et al.* Prion strains depend on different endocytic routes for productive infection. *Sci. Rep.* **7**, 6923 (2017).
10. Sikorska, B., Liberski, P. P., Giraud, P., Kopp, N. & Brown, P. Autophagy is a part of ultrastructural synaptic pathology in Creutzfeldt-Jakob disease: a brain biopsy study. *Int. J. Biochem. Cell. Biol.* **36**, 2563–2573 (2004).
11. Dearmond, S. J. & Bajsarowicz, K. PrPSc accumulation in neuronal plasma membranes links Notch-1 activation to dendritic degeneration in prion diseases. *Mol. Neurodegener.* **5**, 6 (2010).
12. Liberski, P. P., Gajdusek, D. C. & Brown, P. How do neurons degenerate in prion diseases or transmissible spongiform encephalopathies (TSEs): neuronal autophagy revisited. *Acta Neurobiol. Exp.* **62**, 141–147 (2002).
13. Goold, R., McKinnon, C. & Tabrizi, S. J. Prion degradation pathways: potential for therapeutic intervention. *Mol. Cell Neurosci.* **66**, 12–20 (2015).
14. Lawrence, R. E. & Zoncu, R. The lysosome as a cellular centre for signalling, metabolism and quality control. *Nat. Cell. Biol.* **21**, 133–142 (2019).
15. Hu, Y. B., Dammer, E. B., Ren, R. J. & Wang, G. The endosomal-lysosomal system: from acidification and cargo sorting to neurodegeneration. *Transl. Neurodegener.* **4**, 18 (2015).
16. Kopacek, J. *et al.* Upregulation of the genes encoding lysosomal hydrolases, a perforin-like protein, and peroxidases in the brains of mice affected with an experimental prion disease. *J. Virol.* **74**, 411–417 (2000).
17. Zhang, Y., Spiess, E., Groschup, M. H. & Burkle, A. Up-regulation of cathepsin B and cathepsin L activities in scrapie-infected mouse Neuro2a cells. *J. Gen. Virol.* **84**, 2279–2283 (2003).
18. Homma, T. *et al.* Increased expression of p62/SQSTM1 in prion diseases and its association with pathogenic prion protein. *Sci. Rep.* **4**, 4504. https://doi.org/10.1038/srep04504 (2014).
19. Shim, S. Y., Karri, S., Law, S., Schatzl, H. M. & Gilch, S. Prion infection impairs lysosomal degradation capacity by interfering with rab7 membrane attachment in neuronal cells. *Sci. Rep.* **6**, 21658. https://doi.org/10.1038/srep21658 (2016).
20. Price, J. C., Guan, S., Burlingame, A., Prusiner, S. B. & Ghaemmaghami, S. Analysis of proteome dynamics in the mouse brain. *Proc. Natl. Acad. Sci. USA* **107**, 14508–14513 (2010).
21. Claydon, A. J. & Beynon, R. Proteome dynamics: revisiting turnover with a global perspective. *Mol. Cell Proteom.* **11**, 1551–1565 (2012).
22. Cambridge, S. B. *et al.* Systems-wide proteomic analysis in mammalian cells reveals conserved, functional protein turnover. *J. Proteome Res.* **10**, 5275–5284 (2011).
23. Bachmair, A., Finley, D. & Varshavsky, A. Invivo half-life of a protein is a function of its amino-terminal residue. *Science* **234**, 179–186 (1986).
24. Rogers, S., Wells, R. & Rechsteiner, M. Amino-acid-sequences common to rapidly degraded proteins: the pest hypothesis. *Science* **234**, 364–368 (1986).
25. Reverte, C. G., Ahearn, M. D. & Hake, L. E. CPEB degradation during Xenogus oocyte maturation requires a PEST domain and the 26S proteasome. *Dev. Biol.* **231**, 447–458 (2001).
26. Dice, J. F. & Goldberg, A. L. Relationship between invivo degradative rates and isoelectric points of proteins. *Proc. Natl. Acad. Sci. USA* **72**, 3893–3897 (1975).
27. Dice, J. F., Hess, E. J. & Goldberg, A. L. Studies on the relationship between the degradative rates of proteins invivo and their isoelectric points. *Biochem. J.* **178**, 305–312 (1979).
28. Miller, S., Lesk, A. M., Janin, J. & Chothia, C. The accessible surface-area and stability of oligomeric proteins. *Nature* **328**, 834–836 (1987).
29. Klionsky, D. J. & Emr, S. D. Cell: autophagy as a regulated pathway of cellular degradation. *Science* **290**, 1717–1721 (2000).
30. Reichard, E. L. *et al.* Substrate ubiquitination controls the unfolding ability of the proteasome. *Protein Sci.* **25**, 148–149 (2016).
31. Ciechanover, A. Proteolysis: from the lysosome to ubiquitin and the proteasome. *Nat. Rev. Mol. Cell Biol.* **6**, 79–87 (2005).
32. Zhang, T., Shen S., Qu J. & Ghaemmaghami, S. Global analysis of cellular protein flux quantifies the selectivity of basal autophagy. *Cell Rep.* **14**, 2426–2439 (2016).
33. Mathieson, T. *et al.* Systematic analysis of protein turnover in primary cells. *Nat. Commun.* **9**, 689 (2018).
34. Doherty, M. K., Hammond, D. E., Clagule, M. J., Gaskell, S. J. & Beynon, R. J. Turnover of the human proteome: determination of protein intracellular stability by dynamic SILAC. *J. Proteome Res.* **8**, 104–112 (2009).
35. Zhang, T. *et al.* Proteome-wide modulation of degradation dynamics in response to growth arrest. *Proc. Natl. Acad. Sci. USA* **114**, E10329–E10338 (2017).

36. Swovick, K. *et al.* Cross-species comparison of proteome turnover kinetics. *Mol. Cell. Proteom.* **17**, 580–591 (2018).
37. Ghaemmaghami, S., Ullman, J., Ahn, M., St Martin, S. & Prusiner, S. B. Chemical induction of misfolded prion protein conformers in cell culture. *J. Biol. Chem.* **285**, 10415–10423 (2010).
38. Bosque, P. J. & Prusiner, S. B. Cultured cell sublines highly susceptible to prion infection. *J. Virol.* **74**, 4377–4386 (2000).
39. Doh-Ura, K., Iwaki, T. & Caughey, B. Lysosomotropic agents and cysteine protease inhibitors inhibit scrapie-associated prion protein accumulation. *J. Virol.* **74**, 4894–4897 (2000).
40. Korth, C., May, B. C., Cohen, F. E. & Prusiner, S. B. Acridine and phenothiazine derivatives as pharmacotherapeutics for prion disease. *Proc. Natl. Acad. Sci. USA* **98**, 9836–9841 (2001).
41. Levine, D. J. *et al.* Mechanism of scrapie prion precipitation with phosphotungstate anions. *Acs Chem. Biol.* **10**, 1269–1277 (2015).
42. Nagy, G., Tanczos, B., Fidrus, E., Talas, L. & Banfalvi, G. Chemically induced cell cycle arrest in perfusion cell culture. *Methods Mol. Biol.* **1524**, 161–176 (2017).
43. Terao, Y. *et al.* Sodium butyrate induces growth arrest and senescence-like phenotypes in gynecologic cancer cells. *Int. J. Cancer* **94**, 257–267. https://doi.org/10.1002/ijc.1448 (2001).
44. Andriamihaja, M., Chaumontet, C., Tome, D. & Blachier, F. Butyrate metabolism in human colon carcinoma cells: implications concerning its growth-inhibitory effect. *J. Cell Physiol.* **218**, 58–65 (2009).
45. Zhang, T. *et al.* Kinetics of precursor labeling in stable isotope labeling in cell cultures (SILAC) experiments. *Anal. Chem.* **86**, 11334–11341 (2014).
46. Dieterich, D. C., Link, A. J., Graumann, J., Tirrell, D. A. & Schuman, E. M. Selective identification of newly synthesized proteins in mammalian cells using bioorthogonal noncanonical amino acid tagging (BONCAT). *Proc. Natl. Acad. Sci. USA* **103**, 9482–9487 (2006).
47. Ma, Y., McClatchy, D. B., Barkallah, S., Wood, W. W. & Yates, J. R. 3rd. HILAQ: a novel strategy for newly synthesized protein quantification. *J. Proteome Res.* **16**, 2213–2220 (2017).
48. Feng, Y., He, D., Yao, Z. & Klionsky, D. J. The machinery of macroautophagy. *Cell Res.* **24**, 24–41 (2014).
49. Lubke, T., Lobel, P. & Sleat, D. E. Proteomics of the lysosome. *Bba-Mol. Cell. Res.* **1793**, 625–635 (2009).
50. Yoshii, S. R. & Mizushima, N. Monitoring and measuring autophagy. *Int. J. Mol. Sci.* **18**, E1865 (2017).
51. Boellaard, J. W., Kao, M., Schlote, W. & Diringer, H. Neuronal autophagy in experimental scrapie. *Acta Neuropathol.* **82**, 225–228 (1991).
52. Liberski, P. P. *et al.* Ultrastructural characteristics (or evaluation) of Creutzfeldt-Jakob disease and other human transmissible spongiform encephalopathies or prion diseases. *Ultrastruct. Pathol.* **34**, 351–361 (2010).
53. Heiseke, A., Aguib, Y., Riemer, C., Baier, M. & Schatzl, H. M. Lithium induces clearance of protease resistant prion protein in prion-infected cells by induction of autophagy. *J. Neurochem.* **109**, 25–34 (2009).
54. Heiseke, A., Aguib, Y. & Schatzl, H. M. Autophagy, prion infection and their mutual interactions. *Curr. Issues Mol. Biol.* **12**, 87–97 (2010).
55. Safar, J. G. *et al.* Prion clearance in bigenic mice. *J. Gen. Virol.* **86**, 2913–2923 (2005).
56. Chiesa, R., Piccardo, P., Biasini, E., Ghetti, B. & Harris, D. A. Aggregated, wild-type prion protein causes neurological dysfunction and synaptic abnormalities. *J. Neurosci.* **28**, 13258–13267 (2008).
57. McShane, E. *et al.* Kinetic analysis of protein stability reveals age-dependent degradation. *Cell* **167**, 803–815 (2016).
58. Ghaemmaghami, S. *et al.* Cell division modulates prion accumulation in cultured cells. *Proc. Natl. Acad. Sci. USA* **104**, 17971–17976 (2007).
59. Nadtochiy, S. M. *et al.* Potential mechanisms linking SIRT activity and hypoxic 2-hydroxyglutarate generation: no role for direct enzyme (de)acetylation. *Biochem. J.* **474**, 2829–2839 (2017).
60. Walker, E. J., Bettinger, J. Q., Welle, K. A., Hryhorenko, J. R. & Ghaemmaghami, S. Global analysis of methionine oxidation provides a census of folding stabilities for the human proteome. *Proc. Natl. Acad. Sci. USA* **116**, 6081–6090 (2019).

Acknowledgements

Author contributions

The study concept was conceived by C.H. and S.G. Its detailed planning was performed with contribution from all authors. C.H., K.W., and J.H. conducted all experiments. Data analysis was conducted by C.H. The manuscript was written by C.H. and S.G. All authors have given approval to the final version of the manuscript.

Competing interests

The authors declare no competing interests.

Additional information

Supplementary information is available for this paper at https://doi.org/10.1038/s41598-020-67505-5.

Correspondence and requests for materials should be addressed to S.G.

Reprints and permissions information is available at www.nature.com/reprints.

Publisher's note Springer Nature remains neutral with regard to jurisdictional claims in published maps and institutional affiliations.